

Diósi-Penrose criterion for solids and electrical components in quantum superpositions and application to a single-photon detector

Garrett Quandt-Wiese
Schlesierstr. 16
64297 Darmstadt
Germany
garrett@quandt-wiese.de
www.quandt-wiese.de

The Diósi-Penrose criterion is applied to solids in quantum superpositions that are slightly displaced against each other or have different expansions in the superposed states. The calculations take the microscopic mass distribution of the solid's nuclei into account, where the spatial variation of the nuclei is calculated with Debye's model for acoustical phonons. The contribution resulting from the mass concentration in the solid's nuclei can be neglected for displacements larger than ten lattice constants but dominates the superposition's decay for displacements smaller than the spatial variation of the nuclei in the order of a tenth of an Ångström. In this regime, the parameter-free Diósi-Penrose model predicts significantly higher decay rates than the version in which the mass density is averaged. With the results for solids, formulas for the decay of superposed electrical components, as plate capacitors, resistors, wires and piezo actuators, are derived, which are used to analyse how long a single-photon detector can stay in a superposition of a photon-detected and a no-photon-detected state, and how its lifetime shortens when it displaces a mass with a piezo actuator.

Keywords: Diósi-Penrose criterion, solids in quantum superpositions.

1. Introduction

For the assessment and analyses of experimental proposals for measuring wavefunction collapse the so-called Diósi-Penrose criterion is often used [1-9], with which the lifetimes of quantum superpositions can be estimated. The Diósi-Penrose criterion [10,11] is derived from the gravity-based collapse models of Diósi [12,13] and Penrose [14,1], which lead to the same results, apart from the point that in Diósi's model the mass density must be averaged over larger areas.

In this work, the Diósi-Penrose criterion is applied to superposed macroscopic solids, which are in the superposed states slightly displaced with respect to each other or have slightly different expansions. The calculations take the geometry of the solids and the type of displacement between the superposed states into account and regard the solid's microcosmic mass distribution resulting from the mass concentration in its atomic nuclei. The microscopic mass distribution is calculated with Debye's model for acoustical phonons in which the spatial variation of the nuclei increases with temperature. To build a bridge to concrete experiments, the results are applied to

electrical components such as plate capacitors, resistors, wires and piezo actuators, which can evolve into a superposition, when they are e.g. part of a single-photon detector. For such a single-photon detector, it is investigated how long it can stay in a superposition of a *photon-detected* and a *no-photon-detected state*, and how its lifetime shortens when it displaces a mass with help of a piezo actuator in case of a photon detection.

This work is structured as follows. In section 2 we introduce the Diósi-Penrose criterion and discuss in section 2.1 the differences in Diósi's model. In section 3, we develop the Diósi-Penrose criterion for superposed solids step by step. First, we consider solids with uniformly distributed mass (section 3.1), calculate then the additional contribution resulting from the mass concentration in the solid's nuclei (section 3.2), and discuss then both effects (section 3.3). Finally, we show the differences arising in Diósi's model when the mass density must be averaged (section 3.4). In section 4 we apply the results to electrical components and calculate in section 5 the lifetime of a single-photon detector.

2. Diósi-Penrose criterion

At the Diósi-Penrose criterion, the mean lifetime of a superposition T_G can be estimated with a characteristic gravitational energy between the superposed states E_{DP} by:

$$T_G \approx \frac{\hbar}{\gamma E_{DP}}. \quad (1)$$

The energy E_{DP} , which we denote here as the *Diósi-Penrose energy*, depends on the difference of the mass density distributions $\rho_1(\mathbf{x})$ and $\rho_2(\mathbf{x})$ of the superposed states and is given by [15-17,1]:

$$E_{DP} = \frac{G}{2} \int d^3\mathbf{x} d^3\mathbf{y} \frac{(\rho_2(\mathbf{x}) - \rho_1(\mathbf{x}))(\rho_2(\mathbf{y}) - \rho_1(\mathbf{y}))}{|\mathbf{x} - \mathbf{y}|}, \quad (2)$$

where G is the gravitational constant. The factor γ in (1) is a dimensionless factor, which is expected to be of the order of one [1]. In all subsequent calculations, γ is assumed to be one and therefore not listed explicitly.

The Diósi-Penrose energy can also be written as follows, where $\Phi_i(\mathbf{x})$ is the gravitational potential corresponding to the mass distribution $\rho_i(\mathbf{x})$ ($\Phi_i(\mathbf{x}) = - \int d^3\mathbf{y} \frac{\rho_i(\mathbf{y})}{|\mathbf{y} - \mathbf{x}|}$.)

$$E_{DP} = -\frac{1}{2} \int d^3\mathbf{x} (\rho_2(\mathbf{x}) - \rho_1(\mathbf{x}))(\Phi_2(\mathbf{x}) - \Phi_1(\mathbf{x})). \quad (3)$$

From this illustration it follows that the Diósi-Penrose energy is minus the gravitational self-energy resulting from the difference of the mass density distributions $\rho_2(\mathbf{x}) - \rho_1(\mathbf{x})$ of the superposed states. For some calculations it is helpful to write the Diósi-Penrose energy in the following form [1]:

$$E_{DP} = \frac{1}{8\pi G} \int d^3x |g_1(x) - g_2(x)|^2 , \quad (4)$$

where $g_i(x)$ are the gravitational fields resulting from the gravitational potentials $\Phi_i(x)$ ($g_i(x) = -\nabla\Phi_i(x)$). From equation (4) it follows that the Diósi-Penrose energy is always positive.

2.1. Diósi-Penrose model with smeared mass-density operator

An important difference in Diósi's model compared to Penrose's approach is that there is a need to modify the mass-density operator to avoid divergences in the master equation for the evolution of the density matrix. This can be achieved by introducing a characteristic smearing radius R_{sm} for the calculation of the mass density with the mass-density operator $\hat{\rho}(x)$ as follows [12,13]:

$$\hat{\rho}(x) = \sum_i m_i \delta(x - \hat{x}_i) \Rightarrow \hat{\rho}(x) = \sum_i \frac{m_i}{\frac{4\pi}{3} R_{sm}^3} \Theta(R_{sm} - |x - \hat{x}_i|) , \quad (5)$$

where m_i and \hat{x}_i are the mass and the position operator of the i 's particle. The choice of the smearing radius R_{sm} determines how much the total energy of a system increases over time. To avoid unrealistically large increases, it was suggested to choose R_{sm} in the order of 10^{-5} cm [13,18]. From measurements of spontaneous photon emissions in solids, which can be a consequence of the permanent energy increase, it was shown that this radius must be at least larger than 0.5 \AA [19]. Since this is larger than the spatial variation of the solid's nuclei, which will be calculated in section 3.2, the mass density distribution must be calculated in Diósi's model different than in Penrose's. The differences resulting from a smearing of the mass-density operator with $R_{sm} \approx 10^{-5} \text{ cm}$ will be outlined for all results in this paper, where the model without smearing of the mass-density operator will be referred to as the *parameter-free Diósi-Penrose model*.

3. Diósi-Penrose energy of superposed solids

In this section, we calculate the Diósi-Penrose energy of superposed solids that are slightly displaced with respect to each other or have slightly different expansions in the superposed states. The displacements shall always be significantly smaller than the dimensions of the solid, a restriction that is sufficient for most experiments. In section 3.1, we first simplify the calculation by neglecting the microscopic mass distribution resulting from the solid's nuclei by averaging the mass density. In section 3.2, we examine then the additional contribution resulting from the solid's nuclei, and discuss in section 3.3 the total Diósi-Penrose energy of superposed solids. In section 3.4 we look at the differences arising for the Diósi-Penrose model with smeared mass-density operator.

3.1. Contribution when spatially averaging the mass density

In this paper, we consider the four cases for superposed solids shown in figure 1. On the one hand, disks that are slightly displaced with respect to each other, or have slightly different extensions, and on the other hand, a rod that has slightly different extensions in the superposed states.

For the following calculation, we first assume that both the disk and the rod are infinitely extended. Under this assumption, the Diósi-Penrose energy can be calculated with equation (4). The gravitational field $g(x)$ is for the disk then always perpendicular to its plane and for the rod it points away from its centre. With the help

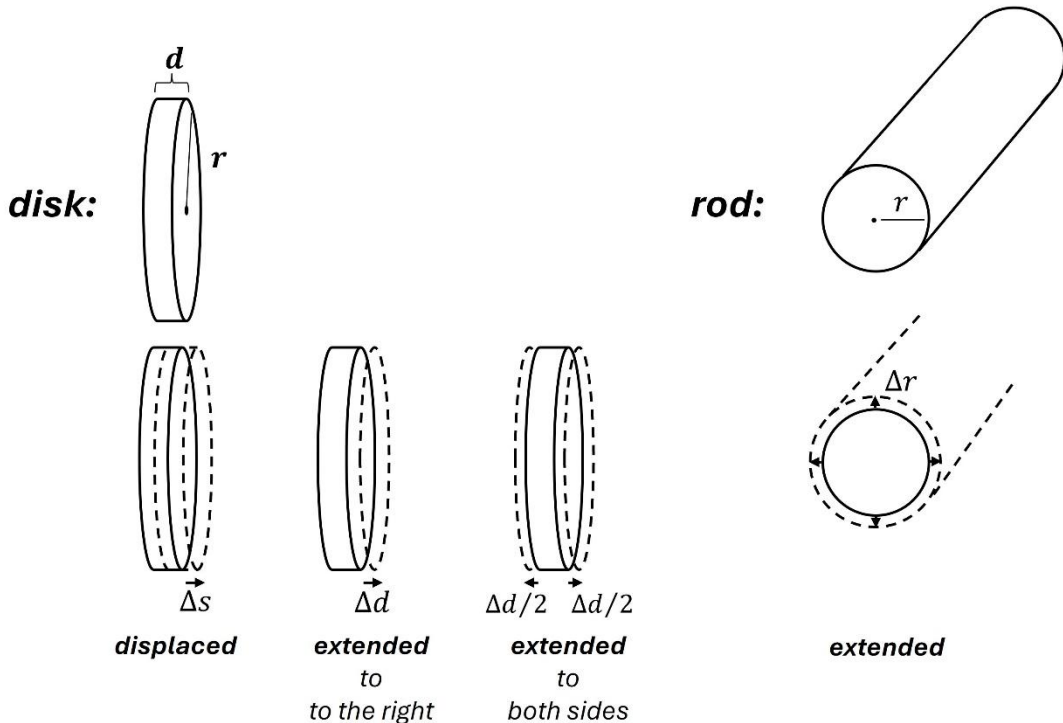


Figure 1. Discussed cases of solids in quantum superpositions. *Left:* Disk that is displaced by Δs in one state relative to the other state or has slightly different thicknesses Δd in the states (e.g. due to compression or piezoelectricity). *Right:* Rod that has slightly different radii r in the states (e.g. due to thermal expansion).

of the law of flux, we obtain for the disk $2g(x) = 4\pi G\rho 2x$, and for the rod: $2\pi r g(r) = 4\pi G\rho\pi r^2$, where x is the distance from the centre of the disk, r the distance from the centre of the rod, and ρ the spatially averaged mass density of the solid. With $x' = x - \Delta s$ and $\rho' = \rho$ for the *displaced disk* (where the dashed variables refer to the second state), $x' = x - \Delta d/2$ and $\rho' = \rho(1 - \frac{\Delta d}{d})$ for the *disk extended to the right*, $x' = x$ and $\rho' = \rho(1 - \frac{\Delta d}{d})$ for the *disk extended to both sides*, and $r' = r$ and $\rho' = \rho(1 - 2\frac{\Delta r}{r})$ for the *extended rod*, we get for displacements, which are much smaller than the size of the solid ($\Delta s, \Delta d \ll d, \Delta r \ll r$), the following result:

$$\begin{aligned}
 E_{DP \bar{\rho}} &= 2\pi GV\rho^2\Delta s^2 && \text{displaced disk} \\
 E_{DP \bar{\rho}} &= \frac{1}{3} 2\pi GV\rho^2\Delta d^2 && \text{disk extended to the right} \\
 E_{DP \bar{\rho}} &= \frac{1}{12} 2\pi GV\rho^2\Delta d^2 && \text{disk extended to both sides} \\
 E_{DP \bar{\rho}} &= \frac{1}{2} 2\pi GV\rho^2\Delta r^2 && \text{extended rod}
 \end{aligned} \tag{6}$$

for: disk and rod infinitely extended ,

where V is the volume of the solid. This result could suggest that the Diósi-Penrose energy of a superposed solid is generally proportional to its volume V , but which is not the case. For example, for a rod being displaced parallel to its direction, the Diósi-Penrose energy does not linearly increase with the rod's length. It converges to a constant value for large lengths of the rod.

In reference [1], the Diósi-Penrose energy was calculated for an oblate-like spheroid that is displaced perpendicular to its plane. For the case of small displacements Δs and radii of the spheroid r_{sph} that are much larger than its thickness s ($\Delta s \ll d, r_{sph} \gg d$), the Diósi-Penrose energy is given by $2\pi GV\rho^2\Delta s^2(1 + \pi d/(4r_{sph}))$, where V is the volume and ρ the mass density of the spheroid. This result converges for $r_{sph} \gg d$, as expected, against the Diósi-Penrose energy of the *displaced disk* (6). If one assumes that the displaced spheroid leads to approximately the same Diósi-Penrose energy as the displaced disk if their thickness and volume are identical, which is the case for $r_{sph} = \sqrt{1.5} r$, then we get for a finite disk with radius r the following correction to our results (6) for infinitely extended disks:

$$\begin{aligned}
 E_{DP \bar{\rho}} &\approx 2\pi GV\rho^2\Delta s^2(1 + 0.64\frac{d}{r}) && \text{displaced disk} \\
 E_{DP \bar{\rho}} &\approx \frac{1}{3} 2\pi GV\rho^2\Delta 2\pi Gd^2(1 + 0.64\frac{d}{r}) && \text{disk extended to the right} \\
 E_{DP \bar{\rho}} &\approx \frac{1}{12} 2\pi GV\rho^2\Delta d^2(1 + 0.64\frac{d}{r}) && \text{disk extended to both sides}
 \end{aligned} \tag{7}$$

3.2. Additional contribution due to the mass concentration in the nuclei

To understand how the Diósi-Penrose energy of the superposed solid changes, when one assumes that its mass is not uniformly distributed but concentrated in its nuclei, the following illustration of the Diósi-Penrose energy is helpful. Assuming hypothetically that the masses of the superposed state 1 and 2 attract each other by the gravitational force, the Diósi-Penrose energy describes the mechanical work to pull the masses of state 1 and 2 apart from each other against this gravitational attraction. This illustration of Diósi-Penrose energy only applies exactly when rigid objects are displaced against each other, as at the *displaced disk* in figure 1. The mechanical work to move the disk in state 2 over the distance Δs in the gravitational potential of state 1 $\Phi_1(\mathbf{x})$ is given by $\int d^3x (\rho_2(\mathbf{x}) - \rho_1(\mathbf{x}))\Phi_1(\mathbf{x})$ and is identical to the mechanical work to move the disk in state 1 in the gravitational potential of state $\Phi_2(\mathbf{x})$, which is given by $\int d^3x (\rho_1(\mathbf{x}) - \rho_2(\mathbf{x}))\Phi_2(\mathbf{x})$. This directly leads to the Diósi-Penrose energy in the form of equation (3). From this illustration, it follows that for small displacements Δs , where the gravitational force can be linearised ($F_G \sim \Delta s$), the Diósi-Penrose energy increases quadratically with the displacement ($E_{DP} \sim \Delta s^2$), which agrees with our calculations in equation (6). The left part of figure 2 illustrates the gravitational forces F_G between all partial masses of the solid in state 1 and 2 when the mass is spatially averaged. The right part of the figure shows the additional forces occurring when the mass of the solid is concentrated in its nuclei. For small displacements, neighbouring atomic nuclei attract each other strongly due to the high mass concentration in the nuclei. For larger displacement, the high mass concentration in the nuclei no longer plays a role, since the force between them does hardly change when the nuclei's masses are evenly distributed over the respective lattice cells. We therefore expect when taking the mass concentration in the nuclei into account that changes to our calculations with averaged mass density only occur for small displacements between the solids, smaller than a few lattice constants.

To calculate the additional contribution to the Diósi-Penrose energy due to the gravitational forces between neighbouring nuclei, we first calculate the Diósi-Penrose energy of a single superposed nucleus, where the mass distribution of the nucleus is

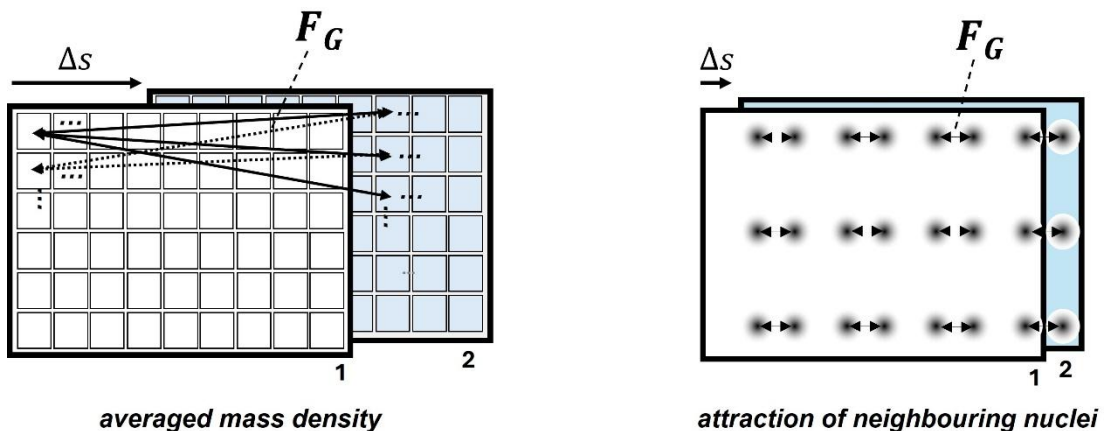


Figure 2. Illustration of the gravitational forces F_G between the two states of a superposed solid displaced by Δs . *Left:* Forces when averaging the mass density of the solid. Here, each partial mass in state 1 attracts each partial mass in state 2, as illustrated in the figure. *Right:* Additional forces due to the mass concentration in the solid's nuclei. Here, strong forces occur between neighbouring nuclei if they are only slightly displaced against each other.

assumed to be Gaussian as follows:

$$\rho(x) = \frac{m}{\sqrt{2\pi} \sigma^3} e^{-\frac{x^2}{2\sigma^2}}. \quad (8)$$

Here m is the nucleus' mass and σ its spatial variation. The Diósi-Penrose energy of such a Gaussian mass distribution being displaced in state 1 and 2 by Δs was calculated for the general case in reference [1] and for the limiting cases $x \ll 1$ and $x > 4$ in the appendix 2 of reference [20]. It leads to the following result:

$$E_{DP} = \frac{Gm^2}{\sqrt{\pi}\sigma} f_\sigma\left(\frac{\Delta s}{\sigma}\right), \quad (9)$$

with

$$f_\sigma(x) = 1 - \frac{\sqrt{\pi}}{x} \operatorname{erf}\left(\frac{x}{2}\right) \approx \begin{cases} \frac{1}{12}x^2 & x \ll 1 \\ 1 - \frac{\sqrt{\pi}}{x} & x > 4 \end{cases}. \quad (10)$$

The course of the function $f_\sigma(x)$ is shown in figure 3. For small displacement ($\Delta s \ll \sigma$), for which the gravitational force between the nuclei in the two states can be linearized ($F_G \sim \Delta s$), one obtains, as expected, a quadratic increase of the Diósi-Penrose energy over the displacement ($E_{DP} \sim \Delta s^2$), and for displacement $\Delta s > 4\sigma$, for which the nuclei in the two states are almost completely separated from each other and the gravitational force decreases with the inverse square of the distance ($F_G \sim 1/\Delta s^2$), the Diósi-Penrose energy converges to a constant value with $1/\Delta s$.

The spatial variation σ of a nucleus in a solid is not of the order of the proton radius ($\approx 10^{-15} m$), but much larger, since the nucleus can oscillate around its rest position due to the excited phonons in the solid. The spatial variation σ can be calculated with

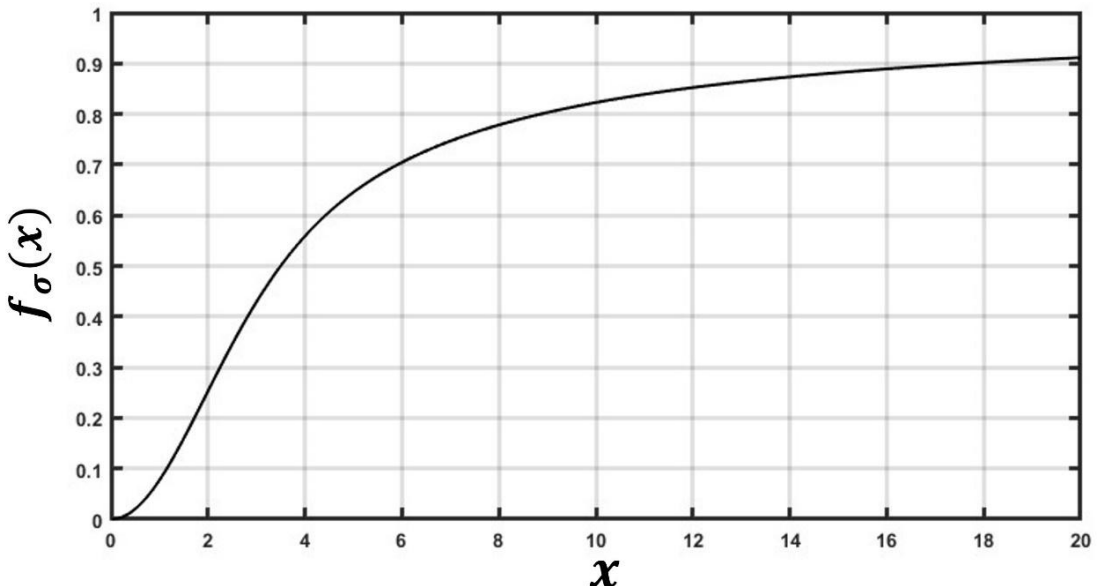


Figure 3. Course of the function $f_\sigma(x)$.

Debye's model for acoustical phonons and leads with the derivation in the [appendix](#) to:

$$\sigma = \sqrt{\frac{3\hbar}{\bar{m} \omega_D^3} \int_0^{\omega_D} d\omega \omega \left(\frac{1}{e^{\frac{\hbar\omega}{k_B T}} - 1} + \frac{1}{2} \right)}, \quad (11)$$

where ω_D is the Debye frequency and \bar{m} the mean atomic mass of the solid, which is defined by:

$$\bar{m} \equiv \sum_i \frac{N_i}{N} m_i. \quad (12)$$

Here N is the total number of atoms and N_i the number of atoms with mass m_i . The Debye frequency ω_D can either be calculated from the solid's Debye temperature θ_D by

$$\hbar \omega_D = k_B \theta_D, \quad (13)$$

which is determined from the temperature profile of the solid's specific heat, or from the sound velocities of the solid, as shown in the [appendix](#). Table 1 shows the spatial variation of the nuclei σ calculated with equations (11) - (13) for selected solids from the parameters on the left for zero and room temperature. These spatial variations are at room temperature typically in the order of a tenth of an Ångström and about a factor of two smaller at zero temperature. The calculated value for copper at zero temperature in table 1 of $\sigma = 0.043\text{\AA}$ agrees precisely with the value reported in reference [18], which was determined from a measurement of the Debye-Waller factor.

To calculate the total Diósi-Penrose energy of a displaced solid, the Diósi-Penrose energies of all nuclei of the solid must be added (see equation (9)):

$$E_{DP\,nucl} = \sum_{nucl\,i} \frac{Gm_i^2}{\sqrt{\pi}\sigma} f_\sigma \left(\frac{\Delta s_i}{\sigma} \right). \quad (14)$$

In this formula the spatial variations σ of all nuclei are assumed to be the same, even if they have different masses as in solids consisting of several chemical elements. This assumption is justified by the fact that in Debye's model the acoustical phonons are relevant for the spatial variation of the nuclei, in which neighbouring atoms oscillate approximately in phase. In approach (14), we assume amorphous solids. In perfect single crystals and displacements by exactly one lattice constant along a lattice axis, there occur strong attractive forces to the neighbouring nuclei of the other state, and the mechanical work to displace the states against each other by one lattice constant would then be zero.

Approach (14) leads for the *displaced disk*, where all neighbouring atomic nuclei are displaced the same distance Δs , to:

$$E_{DP\,nucl} = T_{DP}^{solid} V f_\sigma\left(\frac{\Delta s}{\sigma}\right) \quad \text{displaced disk ,} \quad (15)$$

where the quantity T_{DP}^{solid} is defined by:

$$T_{DP}^{solid} = \frac{G}{\sqrt{\pi}} \frac{\overline{m^2}}{\bar{m}^2} \frac{\bar{g}^3}{\sigma} \rho^2 . \quad (16)$$

Here, \bar{g} is the mean lattice constant of the solid, which can be calculated from the mass density ρ and the mean atomic mass \bar{m} (equation (12)) of the solid by:

$$\bar{g} = \sqrt[3]{\frac{\bar{m}}{\rho}} . \quad (17)$$

The factor $\overline{m^2}/\bar{m}^2$ in (16) is called the *square mass factor* of the solid, which is given by:

$$\frac{\overline{m^2}}{\bar{m}^2} \equiv \frac{\sum_i \frac{N_i}{N} m_i^2}{\bar{m}^2} . \quad (18)$$

For solids consisting of one chemical element the square mass factor is one. For solids consisting of more than one element the term m_i^2 in (18) considers that the Diósi-Penrose energy of a single nucleus is according to equation (9) proportional to the square of its mass.

When calculating the other three cases in figure 1, it must be taken into account that the distances between neighbouring nuclei depends then on the location inside the solid, which leads to the following modification of our result (15):

$$\begin{aligned} E_{DP\,nucl} &= T_{DP}^{solid} V \frac{\int_0^{\frac{\Delta d}{\sigma}} dx f_\sigma(x)}{\frac{\Delta d}{\sigma}} && \text{disk extended to the right} \\ E_{DP\,nucl} &= T_{DP}^{solid} V \frac{\int_0^{\frac{\Delta d}{2\sigma}} dx f_\sigma(x)}{\frac{\Delta d}{2\sigma}} && \text{disk extended to both sides} \\ E_{DP\,nucl} &= T_{DP}^{solid} V \frac{\int_0^{\frac{\Delta r}{\sigma}} 2\pi r dr f_\sigma(r)}{\pi \left(\frac{\Delta r}{\sigma}\right)^2} && \text{extended rod} \end{aligned} \quad (19)$$

For displacements being much larger than the spatial variation of the nuclei, equations (15) and (19) lead for all four cases in figure 1 to the same result¹:

$$E_{DP\,nucl} = T_{DP}^{solid} V \quad \text{for: } \Delta s, \Delta d, \Delta r \gg \sigma . \quad (20)$$

¹ Note that $f_\sigma(x) = 1$ for $x \gg 1$.

	$T = 0 \text{ K}$						$T = 300 \text{ K}$				
	$\rho \left[\frac{g}{\text{cm}^3} \right]$	$\bar{m}[u]$	$\frac{\bar{m}^2}{\bar{m}^2}$	$\bar{g}[\text{\AA}]$	$\theta_D[K]$	$\sigma[\text{\AA}]$	$\frac{T_{DP}^{solid}}{\hbar} \left[\frac{\text{MHz}}{\text{cm}^3} \right]$	ξ	$\sigma[\text{\AA}]$	$\frac{T_{DP}^{solid}}{\hbar} \left[\frac{\text{MHz}}{\text{cm}^3} \right]$	ξ
<i>Al</i>	2.70	26.98	1	2.55	390	0.059	7.3	611	0.105	4.1	106
<i>Si</i>	2.34	28.09	1	2.71	692	0.043	9.0	1844	0.061	6.4	663
<i>Fe</i>	7.87	55.84	1	2.28	373	0.042	62.4	1207	0.077	34.1	197
<i>Cu</i>	8.96	63.55	1	2.28	310	0.043	78.5	1110	0.086	39.3	140
<i>Pb</i>	11.34	207.2	1	3.12	87	0.045	310.1	2504	0.167	83.4	49
<i>Au</i>	19.32	197.0	1	2.57	178	0.032	700.3	3790	0.084	268.4	213
<i>Pt</i>	21.45	195.1	1	2.47	225	0.029	861.6	4736	0.067	370.2	376
<i>SiO₂</i>	2.65	20.03	1.08	2.32	523	0.059	5.8	496	0.093	3.7	127
<i>Al₂O₃</i>	4	20.39	1.07	2.04	980	0.043	12.1	872	0.053	9.7	450
<i>PZT</i> ²	7.6	64.95	2.32	2.42	266	0.046	148.1	2553	0.099	69.0	258

Table 1. Spatial variation of nuclei σ , characteristic Diósi-Penrose energy density T_{DP}^{solid} and the factor ξ , describing how much the Diósi-Penrose energy increases due to the mass concentration in the nuclei for small displacements (see section 3.3) for zero and room temperature calculated for selected solids from their material properties on the left.

The term $T_{DP}^{solid} V$ describes according to the illustration in figure 2 the energy required to pull the nuclei of the solid in the two states far apart from each other against their gravitational attraction. The quantity T_{DP}^{solid} we denoted as the *characteristic Diósi-Penrose energy density* of the solid. The characteristic Diósi-Penrose energy divided by Planck's constant T_{DP}^{solid}/\hbar describes a decay rate per volume (see equation (1)). Table 1 shows T_{DP}^{solid}/\hbar for the selected solids, which are calculated from the parameters on the left in table with equation (16). T_{DP}^{solid}/\hbar ranges from 3.7 MHz/cm^3 for silicon dioxide to 34.1 MHz/cm^3 for iron and 370.2 MHz/cm^3 for platinum at room temperature and is about two times larger at zero temperature.

For displacements much smaller than the spatial variation of the nuclei, where the Diósi-Penrose energy increases quadratically with the displacement, equations (15) and (19) lead with $f_\sigma(x) = \frac{1}{12}x^2$ for $x \ll 1$ to:

$$\begin{aligned}
 E_{DP \text{ nucl}} &= T_{DP}^{solid} V \frac{1}{12} \left(\frac{\Delta s}{\sigma} \right)^2 && \text{displaced disk} \\
 E_{DP \text{ nucl}} &= \frac{1}{3} T_{DP}^{solid} V \frac{1}{12} \left(\frac{\Delta d}{\sigma} \right)^2 && \text{disk extended to the right} \\
 E_{DP \text{ nucl}} &= \frac{1}{12} T_{DP}^{solid} V \frac{1}{12} \left(\frac{\Delta d}{\sigma} \right)^2 && \text{disk extended to both sides} \\
 E_{DP \text{ nucl}} &= \frac{1}{2} T_{DP}^{solid} V \frac{1}{12} \left(\frac{\Delta r}{\sigma} \right)^2 && \text{extended rod}
 \end{aligned} \tag{21}$$

for: $\Delta s, \Delta d, \Delta r \ll \sigma$.

² $Pb(Zr_xTi_{1-x})O_3$ with $x \approx 0.5$.

It is interesting to mention that we get here for the cases in figure 1 the same pre-factors as calculated for solids with averaged mass density in equation (6), namely 1 (*displaced disk*), $\frac{1}{3}$ (*disk extended to the right*), $\frac{1}{12}$ (*disk extended to both sides*) and $\frac{1}{2}$ (*extended rod*).

3.3. Both contributions

In this section we consider both contributions to the Diósi-Penrose energy, the contribution of the nuclei $E_{DP\ nucl}$ and the contribution when spatially averaging the mass density of the solid $E_{DP\ \bar{\rho}}$, and investigate which contribution dominates in which range of displacement. The total Diósi-Penrose energy of a superposed solid is given by the sum of these two contributions:

$$E_{DP} = E_{DP\ \bar{\rho}} + E_{DP\ nucl} \quad , \quad (22)$$

where $E_{DP\ \bar{\rho}}$ is given by (6) or (7) and $E_{DP\ nucl}$ by (15) or (19) for our four cases in figure 1.

For displacement being much smaller than the spatial variation of the nuclei ($\Delta s \ll \sigma$), the contribution of the nuclei $E_{DP\ nucl}$ is by the factor

$$\frac{E_{DP\ nucl}}{E_{DP\ \bar{\rho}}} \equiv \xi = \frac{1}{24\pi^{3/2}} \left(\frac{\bar{m}^2}{m^2} \right) \left(\frac{\bar{g}}{\sigma} \right)^3 \quad \text{for: } \Delta s, \Delta d, \Delta r \ll \sigma \quad (23)$$

larger than the contribution when spatially averaging the mass density $E_{DP\ \bar{\rho}}$, whereby this factor is the same for all cases in figure 1³. Table 1 shows this factor ξ for the selected solids. It ranges from 50 up to 650 at room temperature and is at zero temperature larger (500 - 5000). Since the contribution of the nuclei $E_{DP\ nucl}$ converges for large displacements towards the constant value $T_{DP}^{solid} V$ (equation (20)), the quadratically increasing contribution $E_{DP\ \bar{\rho}}$ (equations (6)) dominates the Diósi-Penrose energy above a certain displacement Δs . For the displaced disk, $E_{DP\ \bar{\rho}}$ reaches $T_{DP}^{solid} V$ for a displacement Δs of:

$$\frac{\Delta s}{\bar{g}} \Big|_{E_{DP\ \bar{\rho}} = T_{DP}^{solid} V} = \sqrt{\frac{1}{2\pi^{3/2}} \left(\frac{\bar{m}^2}{m^2} \right) \frac{\bar{g}}{\sigma}} \quad \text{displaced disk} \quad . \quad (24)$$

For the solids in table 1, $\Delta s/\bar{g}$ ranges from 1.5 to 2.2 at room temperature and from 1.9 to 3.2 at zero temperature. This means that for displacements larger than of about ten lattice constants, the contribution of the nuclei $E_{DP\ nucl}$ to the Diósi-Penrose energy of the solid can be neglected in a good approximation:

$$E_{DP} \approx E_{DP\ \bar{\rho}} \quad . \quad \text{for: } \Delta s, \Delta d, \Delta r > 10\bar{g} \quad (25)$$

³ This follows by dividing equations (21) by equations (6).

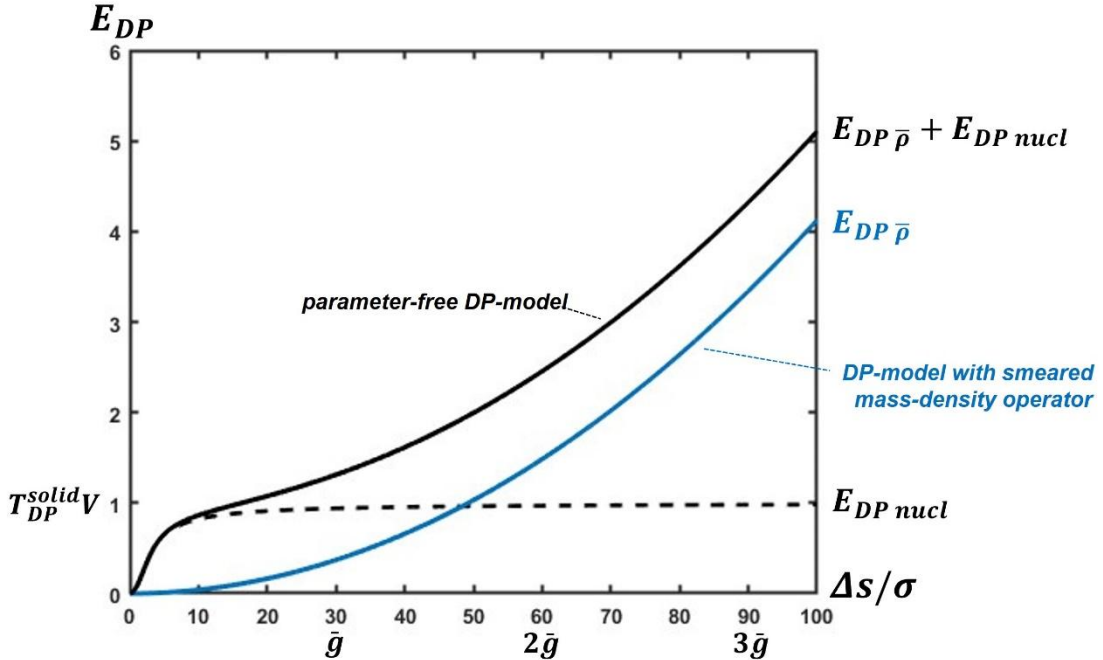


Figure 4. Typical course of the Diósi-Penrose energy of a solid over the displacement Δs (black curve) and of its contributions $E_{DP \bar{\rho}}$ (blue curve) and $E_{DP \text{nucl}}$ (dashed curve) calculated for a solid with $\bar{g}/\sigma = 30$ and $\bar{m}^2/\bar{m}^2 = 1$ and the case of a *displaced disk*.

Figure 4 shows the typical course of the Diósi-Penrose energy of a solid over the displacement Δs (black curve) and of its two contributions $E_{DP \bar{\rho}}$ (blue curve) and $E_{DP \text{nucl}}$ (dashed curve) calculated for a solid with the typical ratio between the mean lattice constant and the spatial variation of its nuclei at room temperature of $\bar{g}/\sigma = 30$ (see values in table 1) and $\bar{m}^2/\bar{m}^2 = 1$ and for the case of a displaced disk. This illustration clearly shows that the contribution of the nuclei $E_{DP \text{nucl}}$ dominates the Diósi-Penrose energy for small displacements and can be neglected for large ones.

3.4. Model with smeared mass-density operator

In this section, we examine how the derived results change when regarding the *Diósi-Penrose model with smeared mass-density operator* in section 2.1. Since the proposed radius for smearing the mass density of $R_{sm} = 10^{-5} \text{ cm}$ (section 2.1) is about 500 times larger than the mean lattice constant \bar{g} of the solids (see table 1), the averaging procedure leads to an almost homogeneous mass distribution, and the Diósi-Penrose energy can be calculated as done in section 3.1 by spatially averaging the mass density and the contribution of the nuclei can be neglected. This leads to:

$$E_{DP} = E_{DP \bar{\rho}} \quad . \quad \text{for: } R_{sm} \gg \bar{g} \quad (26)$$

From the discussion in section 3.3 it follows that for displacements smaller than the spatial variation of the nuclei the *Diósi-Penrose model with smeared mass-density operator* leads to significant smaller decay rates than the parameter-free model,

which are by the factor ξ in table 1 smaller, and that for displacements larger than ten lattice constants both models hardly differ. In figure 4, the course of the Diósi-Penrose energy over the displacement for the *Diósi-Penrose model with smeared mass-density operator* is highlighted as a blue curve.

4. Diósi-Penrose energy of superposed electrical components

In this section, we apply our results for superposed solids to electrical components such as plate capacitors, resistors, wires and piezo actuators. These components can evolve into quantum superpositions when they are part of e.g. a single-photon detector. As we will show in section 5, a single-photon detector can stay for some time in a superposition of a *photon-detected* and a *no-photon-detected state*, and this also applies to its electrical components. For example, in a resistor of the detector a current may have flown in the *photon-detected state* but not in the *no-photon-detected state*, which leads to a warming and thus slight expansion of the resistor in the *photon-detected state*. From this we can calculate with our results for solids a Diósi-Penrose energy for the superposed resistor.

4.1. Plate capacitor

In this section, we consider the plate capacitor in the left of figure 5, to which different voltages V are applied in the two superposed states and consequently the capacitor is charged to different degrees in these states. The main effect that leads to different mass distributions in these states and is therefore relevant for the Diósi-Penrose energy of the superposed capacitor is the compression of its dielectric caused by the electric attraction of its plates. Other effects as the polarization of the dielectric and the different mass densities on the capacitor plates resulting from the charged

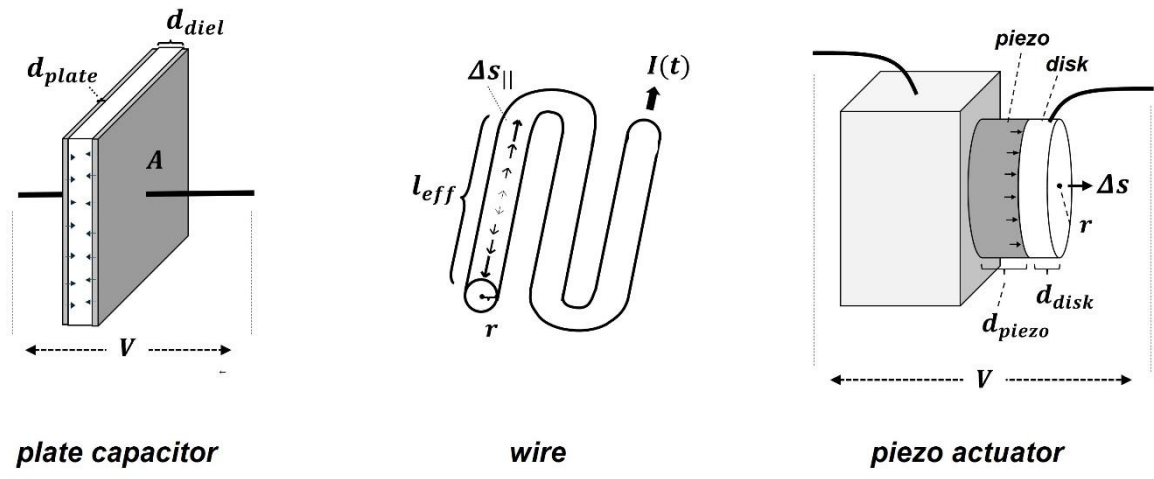


Figure 5. Electrical components discussed in sections 4.1, 4.2 and 4.3.

electrons are orders of magnitude smaller as shown in reference [20].

The compression of the capacitor's dielectric of thickness d_{diel} by Δd_{diel} due to a change of pressure ΔP of the capacitor's plates on the dielectric can be calculated with the modulus of elasticity of the dielectric E_{el} by:

$$\frac{\Delta d_{diel}}{d_{diel}} = -\frac{\Delta P}{E_{el}} . \quad (27)$$

When the voltage V is in one state of the capacitor by ΔV higher than in the other, the dielectric will be compressed in this state by:⁴

$$\Delta d_{diel} = \frac{2\epsilon_0\epsilon_r^2 V \Delta V}{E_{el} d_{diel}} , \quad (28)$$

where ϵ_0 is the electric constant and ϵ_r the dielectric's relative permittivity.

Since this compression of the dielectric is, as the calculations in section 5.1 will show, usually significantly smaller than the spatial variation of the nuclei, the Diósi-Penrose energy of the superposed capacitor is determined for the *parameter-free Diósi-Penrose model* by the contribution of the nuclei only. The Diósi-Penrose energy can then be calculated with equations (21) for the *disk extended to both sides* and the *displaced disk* as⁵:

$$E_{DP} \approx \frac{A}{12} \left(\frac{d_{diel} T_{DP}^{diel}}{12 \sigma_{diel}^2} + \frac{d_{plate} T_{DP}^{plate}}{2 \sigma_{plate}^2} \right) \Delta d_{diel}^2 . \quad \text{parameter-free DP-model} \quad (29)$$

for: $\Delta d_{diel} \ll \sigma$

Here A is the area of the capacitor, d_{diel} and d_{plate} the thicknesses for the capacitor's dielectric and the plates (see figure 5), and σ_{diel} , σ_{plate} , T_{DP}^{diel} and T_{DP}^{plate} their spatial variations of nuclei and characteristic Diósi-Penrose energy densities (16).

Since the contribution of the nuclei is not relevant for the *Diósi-Penrose model with smeared mass-density operator*, the Diósi-Penrose energy of the capacitor must be calculated with equations (6) instead of (21), which leads to:

$$E_{DP} \approx 2\pi G A \left(\frac{1}{12} d_{diel} \rho_{diel}^2 + \frac{1}{2} d_{plate} \rho_{plate}^2 \right) \Delta d_{diel}^2 , \quad \begin{matrix} \text{DP-model with smeared} \\ \text{mass-density operator} \end{matrix} \quad (30)$$

where ρ_{diel} and ρ_{plate} are the mass densities of the dielectric and the plates.

In our results (29) and (30) we simply added the Diósi-Penrose energies resulting from the dielectric and from the two plates of the capacitor together. This is exactly valid for the contribution of the nuclei, i.e. for result (29), but for result (30) only, when the plates of the capacitor are infinitely extended. This can be verified with equation

⁴ This follows with relations $P = F/A$, $F = QE$, $\epsilon_0 AE = Q$, $C = Q/V$ and $C = \epsilon_0 \epsilon_r A/d$, where F is the force between the plates, E the electric field outside the dielectric (which is relevant to calculate the force between the plates), Q the charge on the plates, and C the capacitance.

⁵ Note that the plates are displaced by $\Delta d_{diel}/2$.

(4) as follows. From the law of flux it follows that the difference in the gravitational fields $g_1(\mathbf{x}) - g_2(\mathbf{x})$ belonging to the mass distributions $\rho_1(\mathbf{x})$ and $\rho_2(\mathbf{x})$ in the two states of the superposed dielectric or of the two plates are exactly zero outside the respective component, when they are infinitely extended. Then, when calculating the Diósi-Penrose energy of the plate capacitor with equation (4), the contributions of the dielectric and of the two plates do not interfere and can simply be added.

4.2. Resistors and wires

In this section, we discuss current-carrying components such as resistors and wires. When these components are part of a photon detector, they can differ in the *photon-detected state* and *no-photon-detected state* that in the *photon-detected state* a current $I(t)$ has flowed through them, and in the other state not. A current flow $I(t)$ leads to the following temperature increase of the component:

$$\Delta T = \frac{R}{cM} \int_0^{t_s} dt I(t)^2 , \quad (31)$$

where R is the resistance and M the mass of the component, and c the specific heat of the material. If we consider the wire in the middle of figure 5 exemplary for a current-carrying component, an expansion of the wire leads to displacements of its nuclei at the surface by Δr , but also to displacements $\Delta s_{||}$ along the wire as illustrated in the figure. For the contribution $E_{DP \bar{\rho}}$, when spatially averaging the mass density (section 3.1), only the extension of the rod perpendicular to its surface by Δr is relevant. But, for the contribution of the nuclei $E_{DP \text{nucl}}$ the displacements along the wire $\Delta s_{||}$ are much larger than the perpendicular ones when the length of the wire is much larger than its diameter. For the calculation of $\Delta s_{||}$ only the straight sections of the wire without bending can be used, where the mean length of these straight sections is denoted as effective length l_{eff} as illustrated in figure 5. The change of the wire's radius Δr and of its effective length Δl_{eff} due to a temperature increase ΔT can be calculated with the thermal expansion coefficient of the material α as follows:

$$\begin{aligned} \Delta l_{eff} &= \alpha l_{eff} \Delta T \\ \Delta r &= \alpha r \Delta T \end{aligned} . \quad (32)$$

As for the plate capacitor, the calculations in section 5.1 will show that these displacements are much smaller than the spatial variation of the nuclei ($\Delta l_{eff}, \Delta r \ll \sigma$). For the *parameter-free Diósi-Penrose model*, we must therefore only consider the contribution of the nuclei, where the effect of the displacements of the nuclei parallel to the wire $\Delta s_{||}$ must be calculated with the formula for the *disk extended to both sides* in equation (21), which leads to:

$$E_{DP} \approx \frac{1}{144} T_{DP}^{solid} V \left(\frac{\Delta l_{eff}}{\sigma} \right)^2 \quad . \quad \text{parameter-free DP-model} \quad (33)$$

for: $\Delta l_{eff} \ll \sigma$

For the *Diósi-Penrose model with smeared math-density operator* we get from the extension of the wire's diameter by Δr with equation (6) for the *extended rod* the following result:

$$E_{DP} \approx \pi G V \rho^2 \Delta r^2 \quad . \quad \text{DP-model with smeared mass-density operator} \quad (34)$$

4.3. Piezo actuator

The right part of figure 5 shows a piezo actuator displacing a disk to the right by Δs when a voltage V is applied to it. We regard a piezo for which only the d_{33} -component of the matrix for the converse piezoelectric effect is relevant, where d_{33} describes the extension of the piezo in z-direction when an electrical field E in the same direction is applied ($\Delta d/d = d_{33}E$). Applying a voltage V to the piezo actuator leads then to the following displacement of the disk:

$$\Delta s = d_{33} V \quad . \quad (35)$$

The calculations in section 5.2 for a single-photon detector steering such a piezo actuator yield displacements Δs being larger than ten lattice constants of the solids ($\Delta s > 10\bar{g}$). According to the discussion in sections 3.3 and 3.4 the contribution of the nuclei can be neglected when calculating the Diósi-Penrose energy and the *parameter-free* and the *Diósi-Penrose model with smeared mass-density operator* lead to approximately the same results. With result (7) for the *disk extended to the right* and the *displaced disk* we get for the piezo actuator consisting of the piezo and the disk the following Diósi-Penrose energy:

$$E_{DP} \approx 2\pi G \left(\frac{1}{3} \rho_{piezo}^2 d_{piezo} \left(1 + 0.64 \frac{d_{piezo}}{r} \right) + \rho_{disk}^2 d_{disk} \left(1 + 0.64 \frac{d_{disk}}{r} \right) \right) \pi r^2 \Delta s^2 , \quad (36)$$

for: $\Delta s > 10\bar{g}$

where r is the radius of the disk, d_{piezo} and d_{disk} the thicknesses of the piezo and the disk, and ρ_{piezo} and ρ_{disk} their mass densities.

5. Application to a single-photon detector

In this section, we apply the results derived for electrical components to a single-photon detector and investigate how long it can stay in a superposition of a *photon-detected* and *no-photon-detected state*. In section 5.1 we regard a detector that is decoupled from its environment during detection, and which does not provide any information about the measurement result to the outside during this time. In section 5.2, we investigate how much the detector's lifetime can be shortened when it displaces a mass with a piezo actuator in the case of photon detection.

The upper part of figure 6 shows the setup of the single-photon detector, which detects the photon with a single-photon avalanche photodiode (SPAD) and which operates at room temperature. In the following discussions, we assume that the detection process in the SPAD leads to a superposition of two states, where in one of which an avalanche current has been triggered and in the other it has not. This lets the entire detector evolve into a superposition of a *photon-detected* and *no-photon-detected state*.

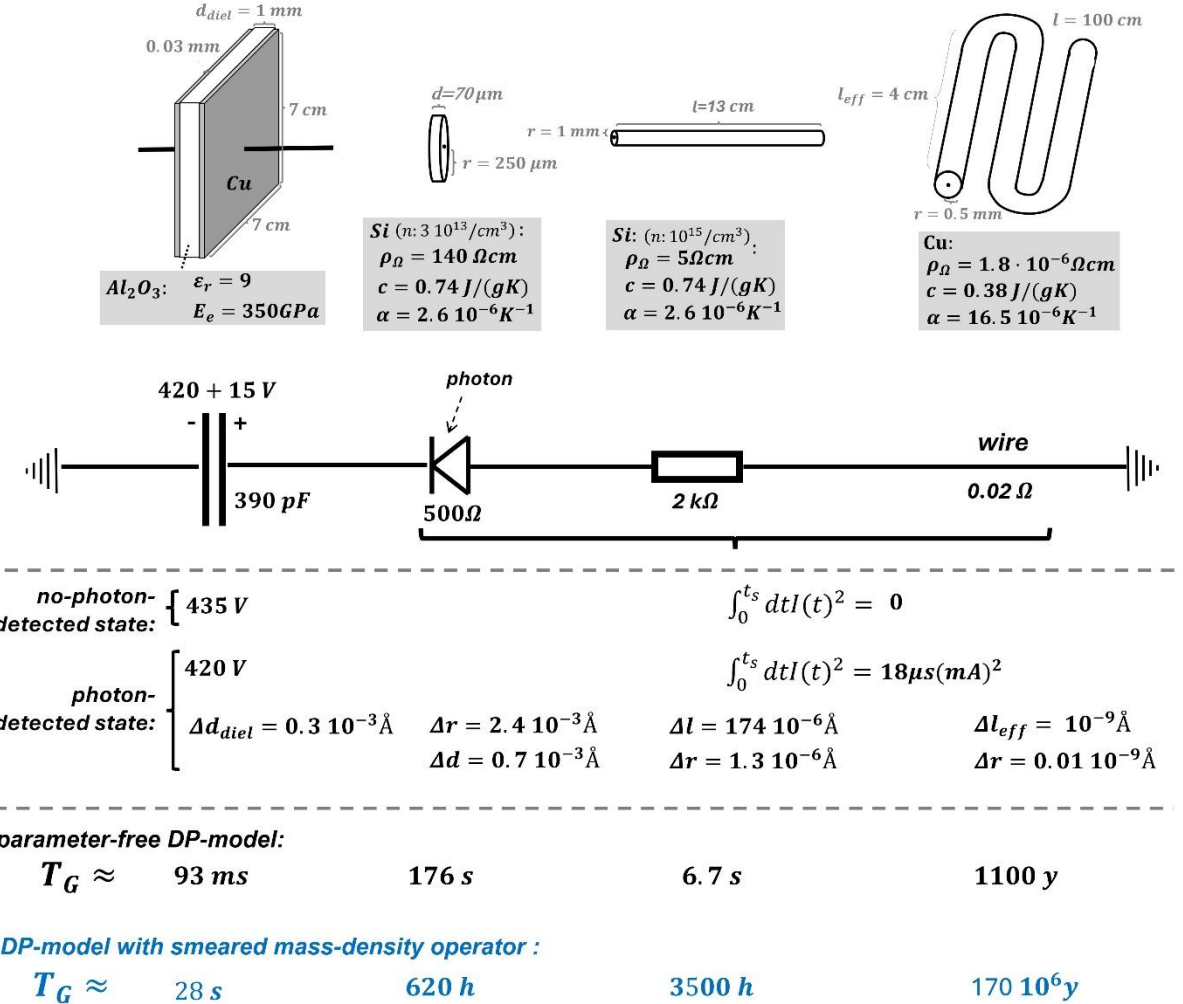
5.1. Detector being decoupled from the environment during detection

For the photodiode in our single-photon detector, we refer to a thick silicon SPAD reported in reference [21] with a breakdown voltage of $V_B = 420\text{ V}$ and an internal resistance of $R_{SPAD} = 500\Omega$. This SPAD detects for an excess bias voltage of $V_E = 15\text{ V}$ photons with wavelengths of 800 nm with a quantum efficiency of 50%. The SPAD is biased with the plate capacitor shown on the left in figure 6 consisting of copper plates and a dielectric of corundum (Al_2O_3). This capacitor is charged shortly before the photon's arrival by a conventional power supply, which will be disconnected from the capacitor during measurement to avoid that this power supply also evolves into a superposition of a *photon-detected* and *no-photon-detected state* and thus shortens the lifetime of the detector. The setup contains a resistor with $R = 2k\Omega$ to slow down the discharge of the plate capacitor by the avalanche current of the SPAD. This resistor shall be realized by a rod of doped silicon with $\rho_\Omega = 5\Omega\text{cm}$ ⁶ as shown in the figure. To be complete, we also consider the wires connecting these components, which are regarded by the 100 cm long copper wire at the right.

When an incoming photon is detected, the following time course of the triggered avalanche current is expected [21]:

$$I(t) = \frac{V_E}{R + R_{SPAD}} e^{-\frac{t}{\tau}} \quad , \quad \text{with } \tau = (R + R_{SPAD}) C \quad (37)$$

⁶ This corresponds to a n-doping concentration of $\approx 10^{15}/\text{cm}^3$.



where C is the capacitance of the plate capacitor. For the parameters in figure 6 the time constant τ is roughly $\tau \approx 1\mu s$. The avalanche current stops when it falls below the latching current of the SPAD of $I_q \approx 0.1mA$ [21], which is at $t_s \approx 3.8\mu s$. At this point in time the voltage at the plate capacitor has dropped from $V_B + V_E = 435 V$ to almost $V_B = 420 V$, and the square of the current flow until this time is $\int_0^{t_s} dt I(t)^2 \approx 18\mu s (mA)^2$. From the voltage drop at the plate capacitor and this current flow through the SPAD, the resistor and the wire, we get with equation (28) for the thickness change of the plate capacitor's dielectric $\Delta d_{dielectric}$, and with equations (31) and (32) for the extensions Δr , Δl and Δl_{eff} of the SPAD⁷, the resistor and the wire the values shown in the middle of figure 6. From these different extensions of the components in the *photon-detected* and the *no-photon-detected state*, we get with the results of sections 4.1 and 4.2 for the Diósi-Penrose energies E_{DP} of the plate capacitor and of

⁷ For the thick silicon SPAD we assume an active area with a radius of $r = 250\mu m$ and a thickness of $d = 70\mu m$ [21], which must have a resistivity of $\rho_\Omega \approx 140\Omega cm$ (this corresponds to a n-doping concentration of $\approx 3 \cdot 10^{13}/cm^3$) to get a resistance of $R_{SPAD} = 500\Omega$.

resistors and wires for the *parameter-free* and the *Diósi-Penrose model with smeared mass-density operator* with $T_G = \hbar/E_{DP}$ (equation (1)) the lifetimes T_G of the components⁸ shown in the lower part of figure 6. The component with the shortest lifetime, which determines the lifetime of the whole detector, is the plate capacitor, which in case of the *parameter-free Diósi-Penrose model* can stay for $T_G \approx 93\text{ms}$, and in the case of the *Diósi-Penrose model with smeared mass-density operator* for even 28s in a superposition.

5.2. Detector displacing a mass with a piezo actuator

In this section, we investigate how the lifetime of our detector shortens when it displaces a mass in case of photon detection. This can be realized with the setup in figure 7, in which the avalanche current of the SPAD charges a piezo actuator, which displaces the copper disk at the right. To simplify discussion, the capacitance C of the plate capacitor biasing the SPAD shall be much larger than the capacitance of the piezo actuator C_{piezo} . Then the voltage course at the piezo actuator is:

$$V_{\text{piezo}}(t) = V_E \left(1 - e^{-\frac{t}{\tau_{\text{piezo}}}}\right) \quad . \quad \text{with: } \tau_{\text{piezo}} = R_{\text{SPAD}} C_{\text{piezo}} \quad (38)$$

For the PZT product *P/C 153* of *PI Ceramic GmbH* [22] we get for the dimensions shown in figure 7 and with the relative permittivity $\epsilon_r = 4200$ of *P/C 153* a capacity of the piezo actuator of $C_{\text{piezo}} = 1300 \text{ pF}$ and a time constant of $\tau_{\text{piezo}} = 0.66 \mu\text{s}$.

Since the piezo actuator will shorten the lifetime of the detector so much that it becomes in the order of the settling time of the detector of $\tau_{\text{piezo}} = 0.66 \mu\text{s}$, the lifetime of the detector cannot be calculated anymore with $T_G = \hbar/E_{DP}$ as in section 5.1, where the lifetimes were much bigger than the detector's settling time and the Diósi-Penrose energy is then approximately constant over the whole lifetime of the detector. To account for a time-varying Diósi-Penrose energy E_{DP} over the detector's lifetime, we must calculate T_G as follows:

$$\int_0^{T_G} dt E_{DP}(t) = \hbar \quad . \quad (39)$$

⁸ For the SPAD in figure 6 (disk with $r = 250\mu\text{m}$ and $d = 70\mu\text{m}$) the Diósi-Penrose energy is calculated for the *parameter-free Diósi-Penrose model* with equation (21) for the *extended rod*, and for the *Diósi-Penrose model with smeared mass-density operator* with equation (6) for the *disk extended to the right*.

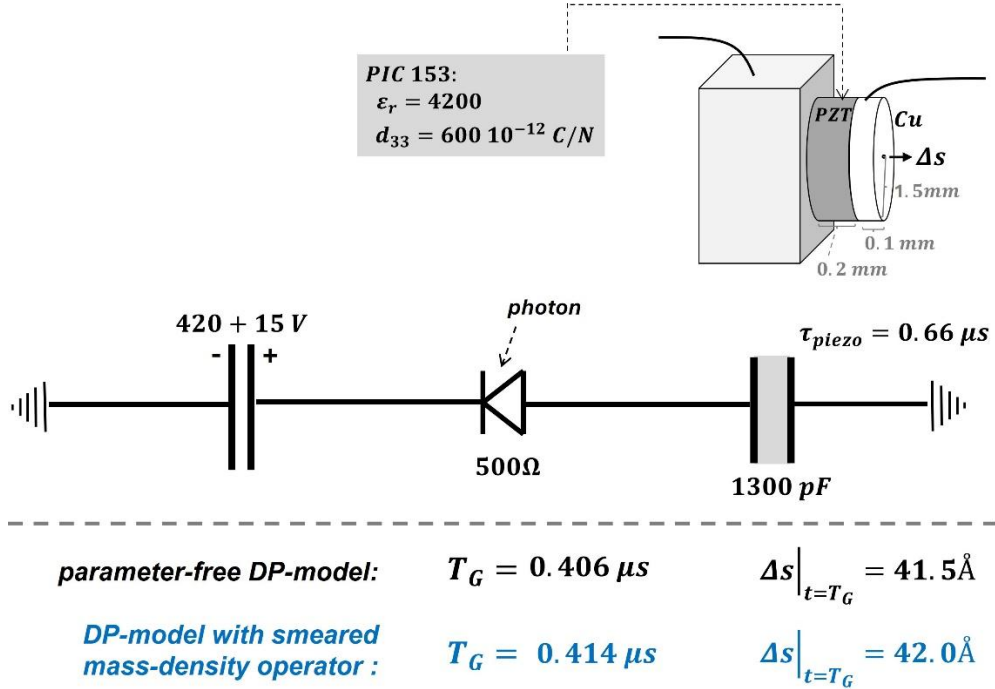


Figure 7. Top: Setup of the single-photon detector displacing a mass (copper disk) with a piezo actuator.

Bottom: Lifetimes of the detector and displacement of the copper disk at $t = T_G$ for the parameter-free and the Diósi-Penrose model with smeared mass-density operator.

With equation (36), which is exactly valid for the *Diósi-Penrose model with smeared mass-density operator*, we obtain a lifetime of $T_G = 0.414 \mu\text{s}$ and a displacement of the copper disc at this time of $\Delta s = 42.0 \text{\AA}$ as shown in figure 7. Taking for the *parameter-free Diósi-Penrose model* additionally the contribution of the nuclei into account (equation (22)), T_G reduces only minimally (see figure 7), since the displacement of $\Delta s = 42 \text{\AA}$ is already larger than ten lattice constants of the used materials (equation (25)).

Finally, we examine how much the lifetime of the photon measurement can be shortened with the piezo actuator in figure 7. By replacing copper with a heavier metal such as gold and increasing the thickness of the disc from 0.1 mm to 0.2 mm , T_G reduces to approximately $T_G \approx 0.2 \mu\text{s}$. To achieve even shorter lifetimes, SPADs with lower internal resistance can be used. For example, with $R_{SPAD} = 175 \Omega$ instead of 500Ω , the lifetime decreases further to $T_G \approx 0.1 \mu\text{s}$. This already approaches the mechanical settling time T of the piezo actuator, which is limited by the sound velocities in PZT and gold ($T \approx d_{\text{piezo}}/\nu_{\parallel \text{PZT}} + d_{\text{disk}}/\nu_{\parallel \text{Au}}$; for $\nu_{\parallel \text{PZT}}$ and $\nu_{\parallel \text{Au}}$ see table 2).

6. Discussion

Our analysis of superposed solids has shown that the *parameter-free* and the *Diósi-Penrose model with smeared mass density operator* differ in the additional contribution to the Diósi-Penrose energy resulting from the mass concentration in the solid's nuclei. This contribution can be neglected for displacements larger than ten lattice constants but dominates for displacements smaller than the spatial variation of the nuclei and leads there to significantly higher decay rates for the *parameter-free* model. With collapse experiments working at such small displacements, it should therefore be possible to distinguish between these models in the future.

Our results for superposed solids, which also apply for solids at very low temperatures, can be used for an analysis of the experimental proposal of Marshall [23], in which a small mirror is transferred into a superposition by the light pressure of a single photon.

Our calculations for piezo actuators displacing masses are of interest for experimental proposals using such components. In reference [24], a piezo actuator was used to reduce the superposition in a Bell experiment over long distances. In the collapse proposal of Tagg et al [25] a Mach-Zehnder interferometer is transferred into a quantum superposition by moving the mirrors of the interferometer with piezo actuators, and in the proposal of the author to test Born's rule at a solid in a three-state superposition [26,27], the solid is transferred in such a superposition with a piezo actuator.

An astonishing result of our calculations is that the single-photon detector being decoupled from the environment can stay for quite a long time in a superposition of the *photon-detected* and the *no-photon-detected state* (about 0.1 s for the *parameter-free* and 30 s for the *Diósi-Penrose model with smeared mass density operator*). This is remarkable since the voltage at the capacitor differs for our example in figure 6 by an amount of 15 V!

The calculations of how long detector components can stay in a superposition are of particular interest for experiments, in which beneath the object of investigation also parts of the setup evolve into superposition, and it therefore becomes necessary to estimate the influence of the setup on the results. This applies to the experiment of Tagg [25] and the experiment proposed by the author [26].

References

- [1] **R. Howl, R. Penrose, I. Fuentes**, Exploring the unification of quantum theory and general relativity with a Bose-Einstein condensate, *New J. Phys.*, 21, 043047 (2019), [arXiv:1812.04630](https://arxiv.org/abs/1812.04630)
- [2] **S. Bose, K. Jacobs, P. L. Knight**, Scheme to probe the decoherence of a macroscopic object, *Phys. Rev. A*, 59, 3204-3210 (1999), [arXiv:quant-ph/9712017](https://arxiv.org/abs/quant-ph/9712017)
- [3] **J. Christian**, Testing gravity-driven collapse of the wavefunction via cosmogenic neutrinos, *Phys. Rev. Lett.*, 95, 160403 (2005), [arXiv:quant-ph/0503001](https://arxiv.org/abs/quant-ph/0503001)
- [4] **J. van Wezel, T. Oosterkamp, J. Zaanen**, Towards an experimental test of gravity-induced quantum state reduction, *Phil. Mag.*, 88, 1005 (2008), [arXiv:0706.3976](https://arxiv.org/abs/0706.3976)
- [5] **O. Romero-Isart**, Quantum superposition of massive objects and collapse models, *Phys. Rev. A*, 84, 052121 (2011), [arXiv:1110.4495](https://arxiv.org/abs/1110.4495)
- [6] **M. Ho, A. Lafont, N. Sangouard, P. Sekatski**, Probing wave function collapse models with a classically driven mechanical oscillator, *New J. Phys.*, 18, 033025 (2016), [arXiv:1504.00790](https://arxiv.org/abs/1504.00790)
- [7] **L. A. Kanari-Naish, J. Clarke, M. R. Vanner, E. A. Laird**, Can the displacement device test objective collapse models?, *AVS Quantum Sci.*, 3, 045603 (2021), [arXiv:2110.15180](https://arxiv.org/abs/2110.15180)
- [8] **R. Kaltenbaek**, Feasibility considerations for free-fall tests of gravitational decoherence, *AVS Quantum Sci.* 4, 015604 (2022), [arXiv:2111.01483](https://arxiv.org/abs/2111.01483)
- [9] **A. Bassi, K. Lochan, S. Satin, T. P. Singh, H. Ulbricht**, Models of wavefunction collapse, underlying theories, and experimental tests, *Rev. Mod. Phys.*, 85, 471-527 (2013), [arXiv:1204.4325](https://arxiv.org/abs/1204.4325)
- [10] **S. L. Adler**, Comments on proposed gravitational modifications of Schrodinger dynamics and their experimental implications, *J. Phys. A*, 40, 755-764 (2007), [arXiv:quant-ph/0610255](https://arxiv.org/abs/quant-ph/0610255)
- [11] **S. Gao**, On Diósi-Penrose criterion of gravity-induced quantum collapse, *Int. J. Theor. Phys.*, 49, 849-853, 2010, [arXiv:1001.4857](https://arxiv.org/abs/1001.4857)
- [12] **L. Diósi**, Models for universal reduction of macroscopic quantum fluctuations, *Phys. Rev. A*, 40, 1165-1174 (1989)
- [13] **G. C. Ghirardi, R. Grassi, A. Rimini**, Continuous-spontaneous-reduction model involving gravity, *Phys. Rev. A*, 42, 1057-1064 (1990)
- [14] **R. Penrose**, On gravity's role in quantum state reduction, *Gen. Rel. Grav.*, 28, 581-600 (1996)
- [15] **S. Donadi, A. Bassi**, Seven non-standard models coupling quantum matter and gravity, *AVS Quantum Sci.*, 4, 025601 (2022), [arXiv:2202.13542](https://arxiv.org/abs/2202.13542)
- [16] **A. Bassi, A. Großardt, H. Ulbricht**, Gravitational decoherence, *Class. Quantum Grav.*, 34, 193002 (2017), [arXiv:1706.05677](https://arxiv.org/abs/1706.05677)

[17] **L. Diósi**, On the conjectured gravity-related collapse rate E_Δ/\hbar of massive quantum superpositions, *AVS Quantum Sci.* 4, 015605-(4) (2022), [arXiv:2111.04604](https://arxiv.org/abs/2111.04604)

[18] **A. Vinante, H. Ulbricht**, Gravity-related collapse of the wave function and spontaneous heating: revisiting the experimental bounds, *AVS Quantum Sci.* 3, 045602 (2021), [arXiv:2109.14980](https://arxiv.org/abs/2109.14980)

[19] **S. Donadi, K. Piscicchia, C. Curceanu, L. Diósi, M. Laubenstein, A. Bassi**, Underground test of gravity-related wave function collapse, *Nature Physics* 17, 74 (2021), [arXiv:2111.13490](https://arxiv.org/abs/2111.13490)

[20] **G. Quandt-Wiese**, Diósi-Penrose criterion for solids in quantum superpositions and a single-photon detector, (2017), [arXiv:1701.00353v3](https://arxiv.org/abs/1701.00353v3)

[21] **S. Cova, S. Ghioni, A. Lacaia, C. Samori, F. Zappa**, Avalanche photodiodes and quenching circuits for single-photon detection, *Applied Optics*, 35(12), 1956-1976 (1996)

[22] **PI Ceramic GmbH**, Catalog on PI Piezoelectric Ceramic Products, <http://www.piceramic.com>

[23] **W. Marshall, C. Simon, R. Penrose, D. Bouwmeester**, Towards quantum superpositions of a mirror, *Phys. Rev. Lett.*, 91, 130401 (2003), [arXiv:quant-ph/0210001](https://arxiv.org/abs/quant-ph/0210001)

[24] **D. Salart, A. Baas, J. A.W. van Houwelingen, N. Gisin, H. Zbinden**, Spacelike Separation in a Bell Test Assuming Gravitationally Induced Collapses, *Phys. Rev. Lett.*, 100, 220404 (2008), [arXiv:0803.2425](https://arxiv.org/abs/0803.2425)

[25] **J. Tagg, W. Reid, D. Carlin**, Schrödinger's Cheshire Cat: A tabletop experiment to measure the Diósi-Penrose collapse time and demonstrate Objective Reduction (OR), (2024), [arXiv:2402.02618](https://arxiv.org/abs/2402.02618)

[26] **G. Quandt-Wiese**, Experimental proposal for the dynamical spacetime approach to wavefunction collapse, (2017), [arXiv:1701.00355](https://arxiv.org/abs/1701.00355)

[27] **G. Quandt-Wiese**, Gravity-induced wavefunction-collapse in a temporally expanding spacetime (2022), [arXiv:1701.01765](https://arxiv.org/abs/1701.01765)

[28] See textbooks on solid state physics, e.g. **K.-H. Hellwege**, Einführung in die Festkörperphysik, *Springer-Verlag, Berlin* (1981)

Appendix

In this appendix we derive equation (11) for the spatial variation of the nuclei in a solid using Debye's model for acoustical phonons. Debye's model assumes the following density of states for the acoustical phonons [28]:

$$D_{Deb}(\omega) = 3N \begin{cases} \frac{3\omega^2}{\omega_D^3} & \omega < \omega_D \\ 0 & \omega > \omega_D \end{cases}, \quad (40)$$

where N is the total number of atoms of the solid and ω_D the Debye frequency. The Debye frequency is related to the Debye temperature θ_D of the solid by $\hbar\omega_D = k_B\theta_D$, where the Debye temperature is determined from the temperature profile of the solid's specific heat. Alternatively, the Debye frequency can be determined from the longitudinal and transverse sound velocities of the solid (v_{\parallel} , v_{\perp}) with [28]:

$$\omega_D^3 = \frac{18\pi^2}{\left(\frac{1}{v_{\parallel}^3} + \frac{2}{v_{\perp}^3}\right)\bar{g}^3} \quad . \quad (41)$$

Table 2 compares the Debye frequencies determined from the Debye temperature $\omega_D(\theta_D)$ with the ones determined from the sound velocities $\omega_D(v_{\parallel}, v_{\perp})$ for the solids in table 1, which differ from each other not more than 20% apart from iron.

The mean energy $\langle E \rangle$ of a single phonon oscillating with frequency ω can be estimated with the Bose-Einstein statistic as:

$$\langle E \rangle = \hbar\omega \left(\langle n \rangle + \frac{1}{2} \right) \quad , \quad \text{with} : \langle n \rangle = \frac{1}{e^{\frac{\hbar\omega}{k_B T}} - 1} \quad . \quad (42)$$

The mean square displacement $\langle x^2 \rangle$ of the atoms oscillating by an excited phonon can be determined from the mean potential energy of the phonon $\langle E_{pot} \rangle = \frac{c}{2} \langle x^2 \rangle$ (where c is the spring constant), and the relation $\langle E \rangle = 2 \langle E_{pot} \rangle$ between the mean energy and the mean potential energy of the phonon. With the relation $\omega^2 = c/M$, where M is the total oscillating mass, which is given by $M = N\bar{m}$, we get:

$$\langle x^2 \rangle = \frac{\langle E \rangle}{N\bar{m}\omega^2} \quad . \quad (43)$$

Taking all excited phonons into account, the mean square displacement of an atom in all three spatial directions is then given by:

$$\langle x^2 + y^2 + z^2 \rangle = \int_0^\infty d\omega D_{Deb}(\omega) \frac{\langle E \rangle}{N\bar{m} \omega^2} . \quad (44)$$

This mean square displacement in all three spatial directions is related to the spatial variation of the nuclei σ by $\langle x^2 + y^2 + z^2 \rangle = 3\sigma^2$ ⁹, which leads directly to our result (11).

⁹ Note that $\int d^3x x^2 \frac{\rho(x)}{m} = 3\sigma^2$ with $\rho(x)$ according to equation (8).

	$\theta_D [K]$	$v_{\parallel}, [\frac{m}{s}]$	$v_{\perp} [\frac{m}{s}]$	$\bar{g} [\text{\AA}]$	$\frac{\omega_D(v_{\parallel}, v_{\perp})}{\omega_D(\theta_D)}$
<i>Al</i>	390	6420	3040	2.55	1.23
<i>Si</i>	692	8433	5843	2.71	1.13
<i>Fe</i>	373	5950	3240	2.28	1.49
<i>Cu</i>	310	4760	2325	2.28	1.32
<i>Pb</i>	87	2160	700	3.12	1.08
<i>Au</i>	178	3240	1200	2.57	1.09
<i>Pt</i>	225	3830	1680	2.47	1.23
<i>SiO₂</i>	523	5800	3700	2.32	1.14
<i>Al₂O₃</i>	980	9542	4368	2.04	0.89
<i>PZT</i>	266	4250	1900	2.42	1.20

Table 2. Comparison of the Debye frequencies calculated from the sound velocities of the solid $\omega_D(v_{\parallel}, v_{\perp})$ with the ones determined from the Debye temperature $\omega_D(\theta_D)$ (see equations (40) and (13)).